

## Study of the Electrochemical Passive-Active Transition of Chalcopyrite in Acidic Solution

Qingyou Liu<sup>1</sup>, Kai Zheng<sup>1, 2</sup>, Xiaoying Wen<sup>1</sup>, Heping Li<sup>1,\*</sup>

<sup>1</sup> Institute of Geochemistry, Chinese Academy of Sciences, Guiyang 550002, China

<sup>2</sup> University of Chinese Academy of Sciences, Beijing, 100039, China

\*E-mail: [liheping123@yahoo.com](mailto:liheping123@yahoo.com)

Received: 28 March 2016 / Accepted: 22 May 2016 / Published: 7 July 2016

---

The electrochemical behaviors of chalcopyrite in 1.0 M H<sub>2</sub>SO<sub>4</sub> were studied by potentiodynamic polarization. The experimental results revealed that chalcopyrite has four different potential ranges: passive for OCP up to 500 mV; trans-passive dissolution/passive from 500 mV to 780 mV; active from 780 mV to 900 mV; and pseudo-passive above 900 mV. When the electrolyte contained 3.0 g/L Fe<sup>3+</sup>, the passive phenomenon weakened markedly, the trans-passive dissolution/passive range became narrower, the active potential sharply decreased, and the electrochemical promoting efficiency increased 34.86-fold. Electrochemical impedance spectroscopy (EIS) confirmed the potentiodynamic results, namely, that chalcopyrite is in a passive state at OCP and its charge transfer resistance  $R_{SC}$  and passive film resistance  $R_p$  are 816.5 and 18,722  $\Omega \cdot \text{cm}^2$ , respectively. At a potential of 800 mV, the chalcopyrite  $R_{SC}$  decreased to 42.9  $\Omega \cdot \text{cm}^2$ , and an equivalent inductance occurred. Passive film did not observed, which was also consistent with the electrode's active characterization. These results have direct implications for chalcopyrite hydrometallurgy.

---

**Keywords:** chalcopyrite; potentiodynamic curve; EIS; electrochemical dissolution

### 1. INTRODUCTION

Chalcopyrite (CuFeS<sub>2</sub>) as one of the most common copper sulfide minerals provides approximately 70% of the world's copper reserves [1]. However, the low leaching rate of chalcopyrite remains problematic because it prevents the full exploitation of chalcopyrite for its low dissolution rate [2]. The major cause of this difficulty arises from the surface passivation of chalcopyrite during electrochemical dissolution. Many studies over the past decades investigating the nature of the passivation have arrived at different conclusions, including the direct oxidation of chalcopyrite to a layer consisting of impermeable sulfur [3], precipitation of iron salts [4], a solid electrolyte interphase

that impedes the rate of charge transfer [5], a metal-deficient sulfide [6], a copper-rich polysulfide layer  $\text{CuS}_x$  [7, 8], and a nonstoichiometric sulfide  $\text{Cu}_{n-1}\text{Fe}_{n-1}\text{S}_{2n}$  [9] or  $\text{Cu}_{1-x}\text{Fe}_{1-y}\text{S}_2$  [10].

In the field of hydrometallurgy, the redox potential deeply affects the leaching response of chalcopyrite to various oxidative solutions. The presence of  $\text{Fe}^{3+}$  as a common oxidizing ion can greatly increase the ore pulp oxidation-reduction potential; thus, it is often used as a leaching medium [11, [12].

In this study, the electrochemical behaviors of chalcopyrite in a 1.0 M  $\text{H}_2\text{SO}_4$  solution with/without 3 g/L  $\text{Fe}^{3+}$  were studied using potentiodynamic polarization, with an aim to characterize chalcopyrite surface properties at different anodic potentials and determine how  $\text{Fe}^{3+}$  ions affect the passive and active transfer of chalcopyrite. Furthermore, EIS tests were performed to confirm the potentiodynamic results and to study the passive and active mechanisms.

## 2. EXPERIMENTAL

### 2.1. Electrode preparation

High-quality natural polycrystalline chalcopyrite was obtained from North Dakota, USA. The chemical composition of this chalcopyrite sample is listed in Table 1.

**Table 1.** Chemical analysis of the chalcopyrite sample

Cu, %	Fe, %	S, %	Ca, %	Zn, %	Pb, %	others, %
33.7	30.8	34.2	<0.01	<0.01	<0.10	1.3

The chalcopyrite sample was cut into approximately cubic samples, and the working areas was  $0.25 \text{ cm}^2$ , trying to avoid visible imperfections. Then, used epoxy resin to seal each specimen, and connected to a copper wire using silver paint on the back face, leaving only the working surface exposed to the solution. Prior to electrochemical test, used no. 1200 carbide paper to polish the working surface to get fresh surface. The electrodes were then degreased by alcohol, rinsed with deionized water, and dried in a stream of air.

### 2.2. Electrochemical measurements

A computer-controlled electrochemical measurement system (PARSTAT2273, Princeton Applied Research) was used to perform the electrochemical measurements. The conventional three-electrode electrolytic cell, namely, the chalcopyrite electrode as working electrode (WE), platinum as auxiliary electrode and saturated calomel electrode (SCE) as reference electrode were adopted.

All potentials quoted in this study are relative to the SCE (242 mV vs. standard hydrogen electrode) unless otherwise noted. A Luggin capillary connected to the SCE was used to minimize the IR drop. The AE and WE were located in separate compartments joined by an anion exchange membrane. The

working, auxiliary and reference electrodes were situated identically to ensure the same spatial relationship in each experiment. To investigate the effect of the  $\text{Fe}^{3+}$  ions, we used two different electrolytes in the working compartment: 1.0 M  $\text{H}_2\text{SO}_4$  and 1.0 M  $\text{H}_2\text{SO}_4$  containing 3.0 g/L  $\text{Fe}^{3+}$ . The experimental temperatures were all  $25 \pm 1^\circ\text{C}$ .

Potentiodynamic curve analysis and EIS were utilized to study the chalcopyrite electrode behaviors. First, the chalcopyrite electrode OCP was measured. The electrochemical experiment was initiated only after the OCP reached a quasi-steady state. Potentiodynamic polarization curves were measured at the potential automatically from -250 to 1000 mV (vs. OCP), and the scan rate was  $0.5 \text{ mV s}^{-1}$ . EIS tests were conducted at different potentials, from 0.01 Hz to 10,000 Hz with a 10 mV AC perturbation. Prior to electrochemical test, each electrode potential was stabilized for 400 seconds. The impedance data were fitted using ZSimpWin 3.20 (2004) software.

### 3. RESULTS AND DISCUSSION

#### 3.1. Open circuit potential study

For many mineral electrodes, the OCP is a mixed potential arising from both the solution and the solid-state redox processes [13]. The open circuit potential of chalcopyrite in 1 M sulfuric acid solution (with/without 3 g/L  $\text{Fe}^{3+}$ ) as a function of time is shown in Figure 1.

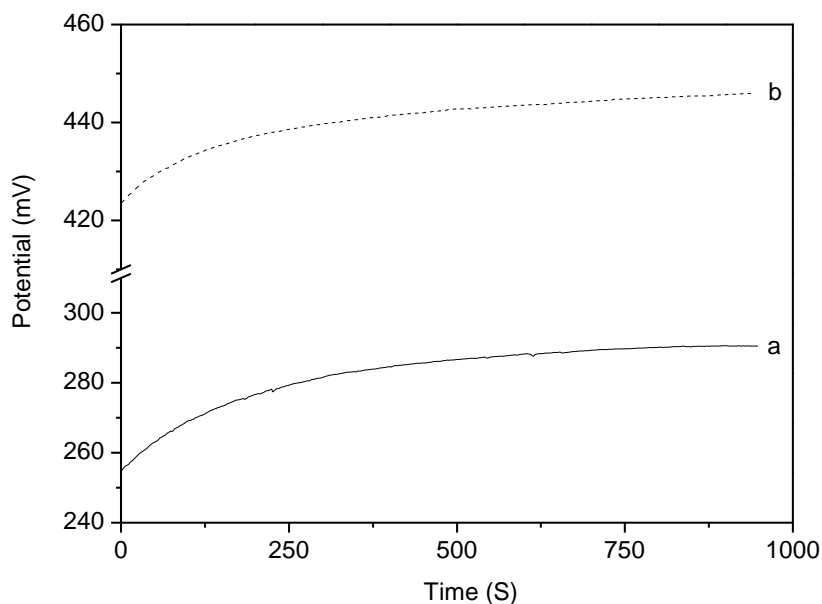
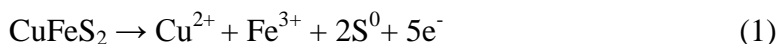


**Figure 1.** Time-potential relationships of chalcopyrite in 1.0 M  $\text{H}_2\text{SO}_4$  (a) and 1.0 M  $\text{H}_2\text{SO}_4$  + 3.0 g/L  $\text{Fe}^{3+}$  electrolyte (b).

In both curves, the chalcopyrite electrode potential increases for approximately 10 min and subsequently reaches a quasi-steady state, indicating a spontaneous passive film grew on the chalcopyrite electrode surface, which can be described by the normal mixed-potential electrochemical

model proposed by Jones and Peters [14] and Miller et al. [15], as shown in Reaction (1). The steady-state OCPs with and without  $\text{Fe}^{3+}$  were found to be approximately  $290.5 \pm 10$  mV and  $445.9 \pm 10$  mV, respectively. The steady-state in this study means the potential varied no more than 2 mV/min. The results revealed that the chalcopyrite OCP is greatly influenced by  $\text{Fe}^{3+}$ . The presence of 3.0 g/L  $\text{Fe}^{3+}$  dramatically increased the value of OCP by increasing the oxide content on the chalcopyrite electrode surface. Specifically, when the electrolyte did not contain  $\text{Fe}^{3+}$ , the cathodic reaction arose from the reduction of dissolved oxygen as reaction (2). However, when the electrolyte contained  $\text{Fe}^{3+}$ , another cathodic reaction as reaction (3) arose. Antonijević et al. [16] pointed out that chalcopyrite potential in solutions of redox components could be defined as:  $E_{\text{CuFeS}_2} = E_{\text{const}} + n \log[\text{Ox}]/[\text{Red}]$ , where  $E_{\text{CuFeS}_2}$  is the chalcopyrite potential, V;  $E_{\text{const}}$  the chalcopyrite potential when  $[\text{Ox}] = [\text{Red}]$ , V;  $n$  the slope of line in system  $E_{\text{CuFeS}_2} = f(\log [\text{Ox}]/[\text{Red}])$ ;  $[\text{Ox}]$  the concentration of oxidized species, M;  $[\text{Red}]$  the concentration of reduced species, M. Obviously, the participation of oxide ions  $\text{Fe}^{3+}$  increasing the  $[\text{Ox}]$ , resulting in more positive  $E_{\text{CuFeS}_2}$ , driving the oxidation of chalcopyrite.



### 3.2. Potentiodynamic curve analysis

Potentiodynamic curves were constructed to determine the surface properties of the chalcopyrite electrode at different anodic potentials and to investigate the effect of  $\text{Fe}^{3+}$ .

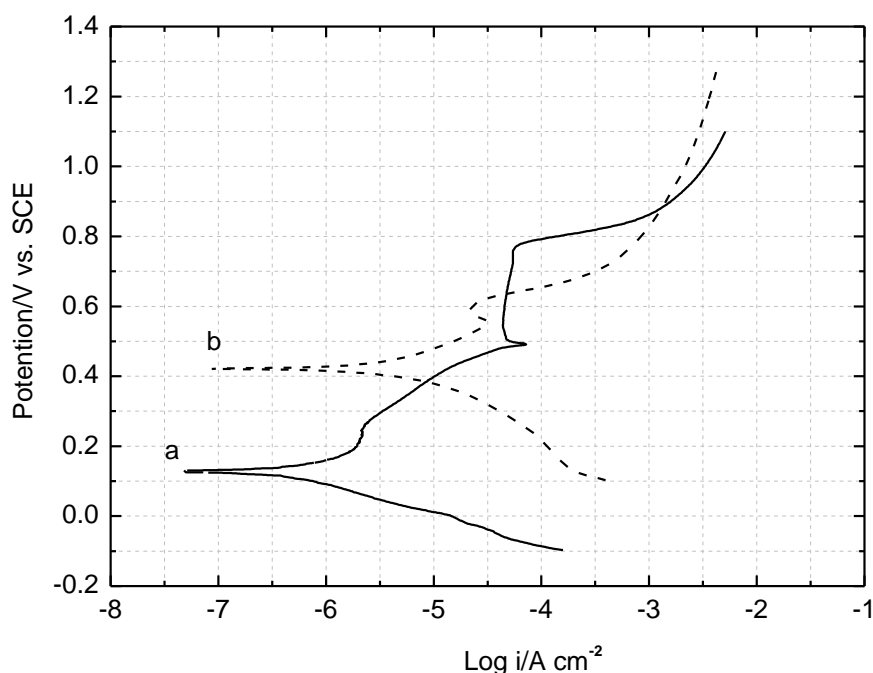


**Figure 2.** Potentiodynamic curves for chalcopyrite electrode in 1.0 M  $\text{H}_2\text{SO}_4$  (a) and 1.0 M  $\text{H}_2\text{SO}_4$  + 3.0 g/L electrolyte (b) at a scan rate of  $0.5 \text{ mV S}^{-1}$ .

Figure 2 shows the potentiodynamic curves for the chalcopyrite electrode in 1.0 M H<sub>2</sub>SO<sub>4</sub> and 1.0 M H<sub>2</sub>SO<sub>4</sub> containing 3.0 g/L Fe<sup>3+</sup>.

The electrochemical parameters of the CuFeS<sub>2</sub> electrode, such as the corrosion current density ( $i_{\text{corr}}$ ) and corrosion potential ( $E_{\text{corr}}$ ), can be measured using the Tafel extrapolation method, which is valid for the sweep rates used in this study, and choosing an extrapolation zone of  $\pm 250$  mV around the  $E_{\text{corr}}$  value after stabilization [17]. In addition, the polarization resistance ( $R_p$ ) can be used in the Stern-Geary equation [18]:  $i_{\text{corr}} = \frac{b_a b_c}{2.3(b_a + b_c)} \cdot \frac{1}{R_p}$ . The detailed electrochemical parameters are shown

in Table 2.

**Table 2.** Electrochemical parameters of CuFeS<sub>2</sub> electrode in different electrolytes

Electrolyte	$E_{\text{corr}}$ (mV)	$i_{\text{corr}}$ ( $\mu\text{A}\cdot\text{cm}^{-2}$ )	$b_a$ (mV)	$b_c$ (mV)	$R_p$ ( $\Omega\cdot\text{cm}^2$ )
1.0 M H <sub>2</sub> SO <sub>4</sub>	106.6	0.25	77.3	221.2	99.6
1.0 M H <sub>2</sub> SO <sub>4</sub> + 3.0 g/L Fe <sup>3+</sup>	421.8	8.96	204.9	424.6	6.7

$E_{\text{corr}}$ : corrosion potential;  $i_{\text{corr}}$ : corrosion current density;

$b_a$ : anode Tafel slope;  $b_c$ : cathode Tafel slope;  $R_p$ : polarization resistance.

When the 1.0 M H<sub>2</sub>SO<sub>4</sub> electrolyte contained 3.0 g/L Fe<sup>3+</sup>, the chalcopyrite corrosion potential  $E_{\text{corr}}$  at 106.6 increased to 421.8 mV, the polarization resistance  $R_p$  at 99.6 decreased to 6.7  $\Omega\cdot\text{cm}^2$ , and the corrosion current density  $i_{\text{corr}}$  at 0.25 increased to 8.96  $\mu\text{A}\cdot\text{cm}^{-2}$ . Note that both of the corrosion potentials are smaller than their OCPs due to the electrochemical parameters determined in the potentiodynamic curves, in which the added different potentials scanned from negative to positive caused cathode “polarization” [8]. These results show that increasing the Fe<sup>3+</sup> content promoted the chalcopyrite electrochemical interaction. The percentage promoting efficiency ( $\eta$ ) was 3486% when the electrolyte contained 3 g/L Fe<sup>3+</sup>; thus, the promoting efficiency increased 34.86 times compared with that without Fe<sup>3+</sup>. In this study,  $\eta$  is defined as  $\eta = \frac{i_{\text{corr}} - i_{\text{corr}}^0}{i_{\text{corr}}^0} \times 100$ , which is often used as the

inhibition efficiency in material science [19, 20]. This phenomenon results from the presence of 3.0 g/L Fe<sup>3+</sup> in the electrolyte changing the cathode reaction from the reduction of dissolved oxygen (Reaction 2) to the reduction of Fe<sup>3+</sup> (Reaction 3). It is well known that the dissolved oxygen content is low (8.0 ~ 8.5 mg/L) at room temperature; thus, the limited current density of the cathode and the corrosion current density of the galvanic cell would be small. However, Fe<sup>3+</sup> has a strong oxidizability; therefore, the existence of Fe<sup>3+</sup> would greatly enhance the cathode reaction.

In the chalcopyrite polarization curve in 1.0 M H<sub>2</sub>SO<sub>4</sub>, we can observe four different potential ranges, and the detailed potential ranges are provided in Table 3.

Furthermore, a comparison of the potentiodynamic curve of the chalcopyrite electrode in 1.0 M H<sub>2</sub>SO<sub>4</sub> with the 3.0 g/L Fe<sup>3+</sup> electrolyte revealed the following: (1) no obvious passive phenomenon occurred during the slow potentiodynamic scan; (2) the trans-passive dissolution/passive area was much narrower (approximately 60 mV) than in the absence of Fe<sup>3+</sup> (280 mV); (3) the active potential was much lower (580 mV) than in the absence of Fe<sup>3+</sup> (780 mV).

**Table 3.** Electrochemical reaction on the surface of chalcopyrite electrode in differential intervals

Surface condition	Potential (mV vs. SCE)	Reaction	Ref.
passive	OCP-500	$CuFeS_2 + 4H_2O \rightarrow Cu_{1-x}Fe_{1-y}S_2 + xCu^{2+} + yFe^{3+} + zSO_4^{2-} + 8zH^+ + (2x + 3y + 6z) e^-$ and/or $CuFeS_2 \rightarrow Cu_{1-x}Fe_{1-y}S_2 + xCu^{2+} + yFe^{2+} + 2(x + y) e^- \quad y \gg x$	(Hackl et al., 1995) (Nava and González, 2006)
Transpassive dissolution/passive	500-780	$Cu_{1-x}Fe_{1-y}S_2 \rightarrow Cu_{1-x-z}S_2 + zCu^{2+} + (1-y)Fe^{2+} + 2(z+1-y) e^-$	(Hackl et al., 1995)
Active	780-900	$Cu_{1-x-z}S_2 \rightarrow (1-x-z)Cu^{2+} + 2S^0 + 2(1-x-z)e^-$ and $CuFeS_2 + 8H_2O \rightarrow Cu^{2+} + Fe^{3+} + 2SO_4^{2-} + 16H^+ + 17e^-$ and/or $CuFeS_2 + 3H_2O \rightarrow Cu^{2+} + Fe^{2+} + S_2O_3^{2-} + 6H^+ + 8e^-$	(Hackl et al., 1995) (Biegler, 1977) (Lazaro and Nicol, 2006)
Pseudo-passive	>900	$2CuFeS_2 + 13H_2O \leftrightarrow 0.75CuS \downarrow + 1.25Cu^{2+} + Fe_2(SO_4)_3 + 0.25SO_4^{2-} + 26H^+ + 28 e^-$	(Nava and González, 2006)

3.3. Electrochemical impedance spectroscopy study

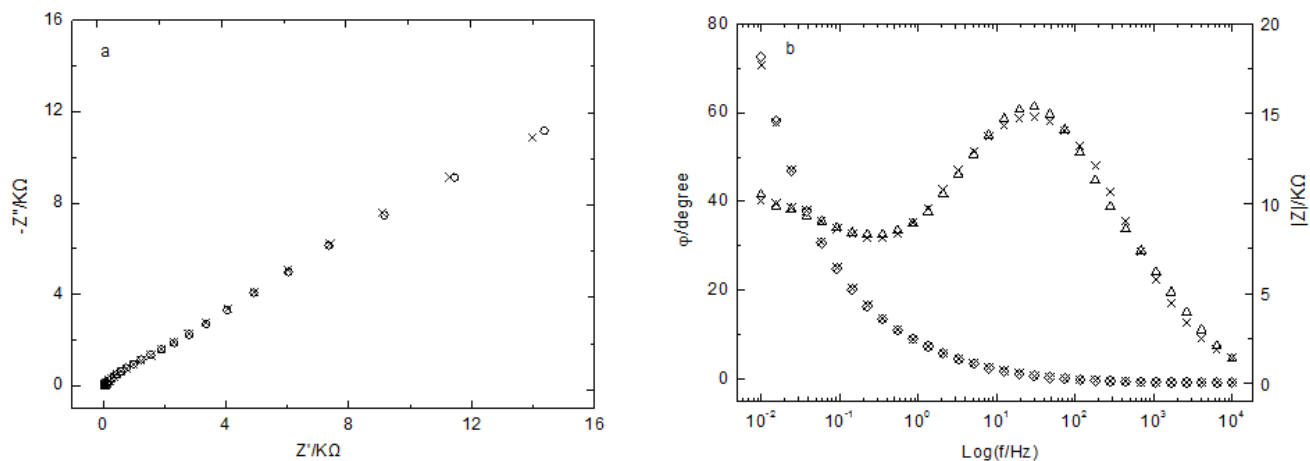


**Figure 3.** Nyquist (a) and Bode (b) plots for the chalcopyrite electrode in 1.0 M H<sub>2</sub>SO<sub>4</sub> at an open circuit potential. (○, Δ and ◇) represent the experimental values, (×) represents simulated values, (Δ) represents the angle degree, and (◇) is the modulus in Figure (3b).

In this section, EIS data for the chalcopyrite electrode in 1.0 M H<sub>2</sub>SO<sub>4</sub> were studied to reveal the chalcopyrite electrochemical interaction mechanism at the passive and active potential areas, and nonlinear method was adopted to fit the equivalent electrochemical circuits (EECs) model parameters [21].

Figure 3 shows the Nyquist and Bode plots for the chalcopyrite electrode at the OCP. The Bode plots in Figure 3b show two capacitive loops. At high frequencies, the loop is attributed to the charge

transfer resistance  $R_{SC}$  in the space charge region, corresponding to the resistance between the chalcopyrite and the outer Helmholtz plane, and at low frequencies, is a slightly distorted capacitive loop, which related to the combination of a pseudo-capacitance impedance (due to the passive layer) and the resistance  $R_p$ . Generally, frequency dispersion or inhomogeneity of the passive layer surface is the causes for the deviation from an ideal semicircle [22]. EEC shown in Figure 4 can be used to characterize the chalcopyrite/electrolyte interface at OCP.

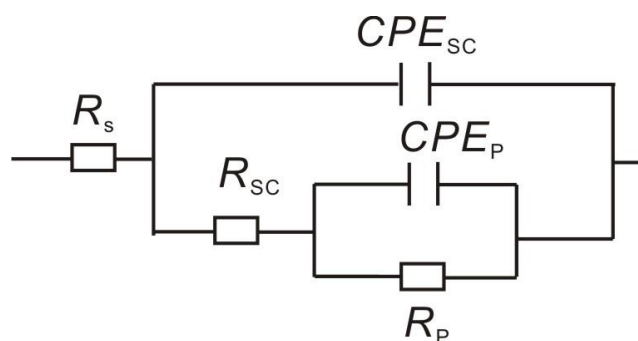


**Figure 4.** Equivalent circuit for chalcopyrite at OCP.

Here and in the following active model,  $R_s$  represents the electrolyte and other ohmic resistances in the respective electrochemical circuit,  $CPE_{SC}$  is a constant phase element corresponding to the space charge region capacitance,  $R_{SC}$  is the charge transfer resistance in the space charge region, and the  $CPE_p/R_p$  pair represents the capacitive and resistive behavior of the passive film. At this potential, the film is believed to be  $Cu_{1-x}Fe_{1-y}S_2$  [7, 23]. In this study, the impedance of  $CPE$  is given by [13]:

$$Z_{CPE} = \frac{1}{Y_0(j\omega)^n}$$

where  $Z_{CPE}$  is the impedance of the constant phase element ( $\Omega \cdot cm^2$ ),  $\omega$  is the angular

frequency of the AC voltage ( $rad \cdot s^{-1}$ ),  $Y_0$  is the magnitude of admittance of  $CPE$  ( $\Omega^{-1} \cdot cm^{-2} \cdot s^{-n}$ ), and  $n$  is the exponential term. The values of the different elements in the equivalent circuit of OCP are shown in Table 4.

**Table 4.** Model parameters for equivalent circuit of Fig. 4

$CPE_{sc}, Y_0 (S \cdot cm^{-2} \cdot s^{-n})$	$n$	$R_{sc} (\Omega \cdot cm^2)$	$CPE_p, Y_0 (S \cdot cm^{-2} \cdot s^{-n})$	$n$	$R_p (\Omega \cdot cm^2)$
$3.17 \times 10^{-4}$	0.65	816.5	$7.22 \times 10^{-4}$	0.54	18722

The space charge transform resistance  $R_{SC}$  and passive film resistance  $R_p$  are 816.5 and 18722  $\Omega \cdot cm^2$ , respectively, indicating a small charge transfer resistance followed by a large passive resistance. These results confirmed that the oxidation of chalcopyrite can occur easily at first and is then prevented by the formation of a passive film at the OCP.

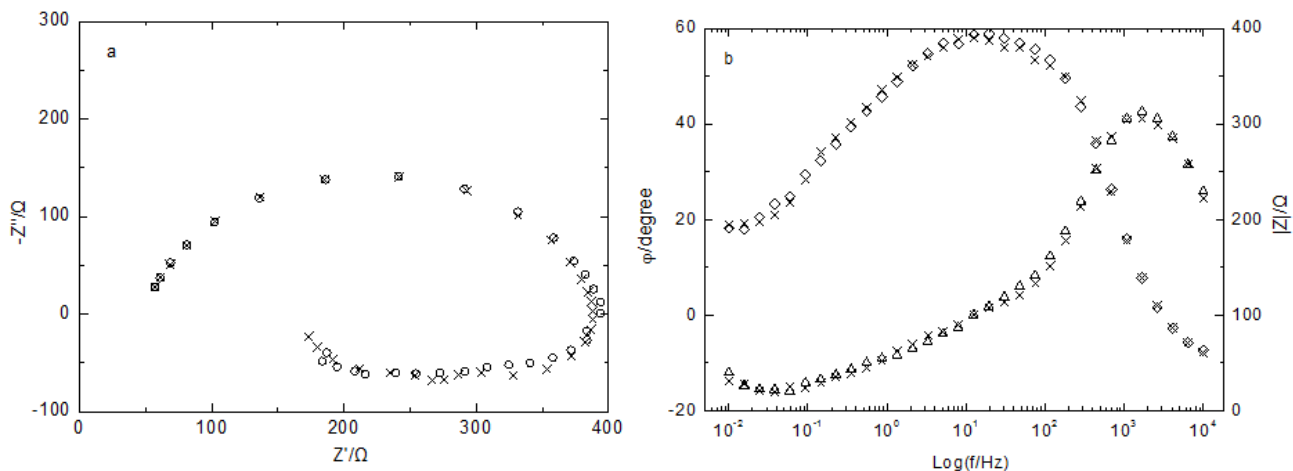


**Figure 5.** Nyquist (a) and Bode (b) plots for the chalcopyrite electrode in 1.0 M H<sub>2</sub>SO<sub>4</sub> at 800 mV. (○, Δ and ◇) represent the experimental values, (×) represents the simulated values, (Δ) represents the angle degree, and (◇) is the modulus in Figure (5b).

Figure 5 shows the Nyquist and Bode plots for chalcopyrite at the anodic potential of 800 mV. The Bode plots show two time constants: the first, at high frequencies, is a capacitive loop related to the combination with a charge transfer resistance, and the second, at middle-low frequencies, is an inductance loop related to the ions relaxation process and a resistance. This trend is in accordance with electrode’s active character.

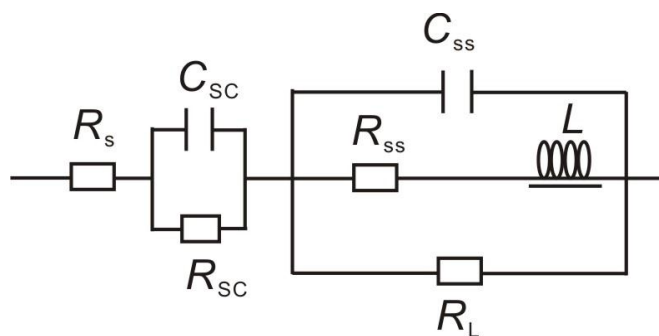


**Figure 6.** Equivalent circuit for chalcopyrite at the active potential.

The equivalent circuit shown in Figure 6 was employed to fit the experimental data where the  $C_{sc}/R_{sc}$  pair represents the charge transfer capacitive and resistive behaviors in the space charge region, respectively. Ghahremaninezhad et al. [10] even used this equivalent circuit to simulate chalcopyrite activity area. The  $C_{ss}||R_L||(LR_{ss})$  section of the model represents the dissolution of the semiconductor electrodes in which  $C_{ss}$  and  $R_{ss}$  contribute to the surface (or interface) states on the electrode,  $R_L$  corresponds to the resistance associated with the accumulation of superficial species, and the element  $L$  is an equivalent inductance, which may be the transfer of ions across the double layer. The values of the different elements in the equivalent circuit of 800 mV are shown in Table 5.

**Table 5.** Model parameters for equivalent circuit of Fig. 6

$C_{sc}$ (F·cm <sup>-2</sup> )	$R_{sc}$ (Ω·cm <sup>2</sup> )	$C_{ss}$ (F·cm <sup>-2</sup> )	$L$ (H·cm <sup>-2</sup> )	$R_{ss}$ (Ω·cm <sup>2</sup> )	$R_L$ (Ω·cm <sup>2</sup> )
$4.94 \times 10^{-6}$	42.9	$4.79 \times 10^{-6}$	1520	38.9	69.2

$R_{sc}$ ,  $R_L$  or  $R_{ss}$  have values no higher than 70 Ω·cm<sup>2</sup>; these low resistance values indicate the electrode's active character. Compared with the OCP parameters, the space charge transfer resistance  $R_{sc}$  of 816.5 Ω·cm<sup>2</sup> decreased sharply to 42.9 Ω·cm<sup>2</sup>, revealing that the electrochemical dissolution of chalcopyrite significantly improved when the added potential from OCP was converted into an active potential.

#### 4. CONCLUSIONS

The electrochemical behaviors of chalcopyrite in a 1.0 M H<sub>2</sub>SO<sub>4</sub> solution were studied using polarization curve analysis and EIS. Two conclusions can be drawn from this research:

(1) The potentiodynamic polarization results revealed that chalcopyrite has four different potential ranges: passive for OCP up to 500 mV; trans-passive dissolution/passive from 500 mV to 780 mV; active from 780 mV to 900 mV; and pseudo-passive above 900 mV. When the electrolyte contained 3.0 g/L Fe<sup>3+</sup>, the passive phenomenon was markedly weaker, the trans-passive dissolution/passive area became narrower, the active potential decreased sharply, and the electrochemical promoting efficiency increased 34.86-fold.

(2) The EIS results confirmed that chalcopyrite was in a passive state at the OCP, and its charge transfer resistance  $R_{sc}$  and passive film resistance  $R_p$  were 816.5 and 18722 Ω·cm<sup>2</sup>, respectively. At 800 mV,  $R_{sc}$  decreased to 42.9 Ω·cm<sup>2</sup>, and passive resistance was not observed, which is consistent with an active character.

#### ACKNOWLEDGEMENTS

This work was financially supported by the 135 Program of the Institute of Geochemistry, CAS, the Key Technologies R & D Program of Guizhou Province, China (SY[2011]3088), and the 863 High Technology Research and Development Program of China (2010AA09Z207).

#### References

1. Y. Li, G. Qian, J. Li and A.R. Gerson, *Geochim. Cosmochim. Acta*, 161 (2015) 188-202.
2. G. Viramontes-Gamboa, B.F. Rivera-Vasquez and D.G. Dixon, *J. Electrochem. Soc.*, 154 (2007) C299-C311.
3. J.E. Dutrizac, *Metall. Trans. B.*, 9B (1978) 431-439.
4. P.B. Munoz, J.D. Miller and M.E. Wadsworth, *Metall. Trans. B.*, 10B (1978) 149-158.
5. R.S. McMillan, D.J. Mackinnon and J.E. Dutrizac, *J. Appl. Electrochem.*, 12 (1982) 743-757
6. H.G. Linge, *Hydrometallurgy*, 2 (1976) 51-64.
7. R.P. Hackl, D.B. Dreisinger, E. Peters and J.A. King, *Hydrometallurgy*, 39 (1995) 25-48.

8. S.L. Harmer, J.E. Thomas, D. Fornasiero and A.R. Gerson, *Geochim. Cosmochim. Acta*, 70 (2006) 4392-4402.
9. E.M. Arce and I. González, *Int. J. Miner. Process.*, 67 (2002) 17-28.
10. A. Ghahremaninezhad, E. Asselin and D.G. Dixon, *Electrochim. Acta.*, 55 (2010) 5041-5056.
11. Y. Yang, W.H. Liu and M. Chen, *Miner. Eng.*, 70 (2015) 99-108.
12. G.K. Yue and E. Asselin, *Electrochim. Acta.*, 146 (2014) 307-321.
13. J.R. Macdonald, *J. Appl. Phys.*, 58 (1985) 1971-1978.
14. D.L. Jones and E. Peters, The leaching of chalcopyrite with ferric sulphate and ferric chloride. In: Yannopoulos, J.C., Agarwaal, J.C. (Eds.), *Extractive Metallurgy of Copper*. AIME, New York (1976).
15. J.D. Miller, P.J. McDonough and H.Q. Portillo, Electrochemical model in silver catalysed ferric sulfate leaching of chalcopyrite. In: Laskowski, J. (Ed.), *13th International Mineral Processing Congress*. Elsevier, Amsterdam (1981).
16. M.M. Antonijević, R. Mihajlović and B. Vukanović, *J. Serb. Chem. Soc.*, 59 (1994) 329.
17. R.G. Kelly, In: R.G. Kelly, J.R. Scully, D.W. Shoesmith, R.G. Buchheit (Eds.), *Electrochemical Techniques in Corrosion Science and Engineering*, Marcel Dekker, Inc., New York (2003).
18. M. Stern and A.L. Geary, *J. Electrochem. Soc.*, 104 (1957) 56-63.
19. R. Solmaz, G. Kardas, B. Yazici and M. Erbil, *Colloid. Surf. A-Physicochem. Eng. Asp.*, 312 (2008) 7-17.
20. X.M. Wang, H.Y. Yang and F.H. Wang, *Corros. Sci.*, 53 (2011) 113-121.
21. J.J. Giner-Sanz, E.M. Ortega and V. Pérez-Herranz, *Electrochim. Acta.*, 186, 20 (2015) 598-612.
22. Q.L. Liu, L.Y. Wang, K. Zheng and H.P. Li, *Ionics*, 21 (2015) 749-753.
23. D. Nava and I. González, *Electrochim. Acta.*, 51 (2006) 5295- 5303.